Estimating nucleation kinetics in a microfluidic setup with and without laser

Thomas Dubbelman

4753380

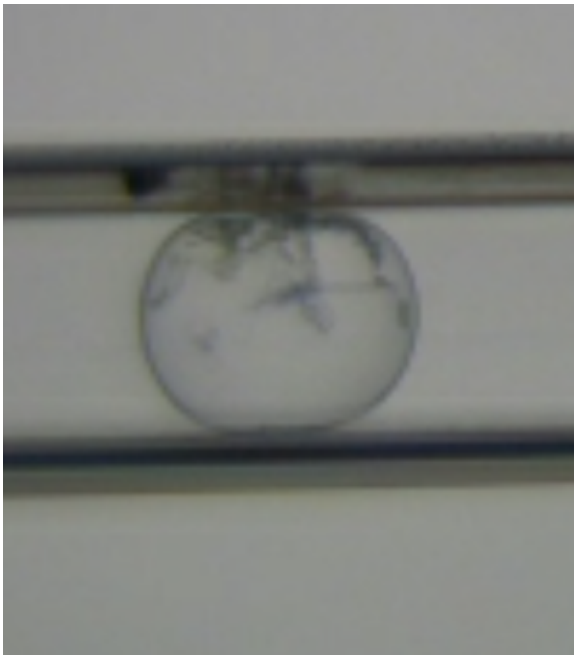

TU Delft

Estimating nucleation kinetics in a microfluidic setup with and without laser

Thomas Dubbelman

4753380

A thesis presented for the degree of
Master of Science

Supervisors: Dr. H.B. Eral
Vikram Korede

Thesis comittee: Dr. H.B. Eral
To be determined
To be determined

ChemE - Faculty of applied sciences & 3ME - Process & Energy
TU Delft
Netherlands
Date of submission: 06-07-2023

Abstract

Crystallization is one of the most common separation techniques in chemical industry. Nonetheless, the nucleation step in the crystallization process is little understood. This makes it difficult to gain control over the crystallization process and more specifically crystal properties. Nucleation mechanics is therefore studied thoroughly. Non-Photochemical Laser-Induced Nucleation has shown to be a promising technique for getting a hold on nucleation and with that crystal properties such as crystal shape, size and morphology. Althoug Non-photochemical Laser-Induced Nucleation is promising, its mechanism has not yet been uncovered and thus requires subsequent research. This research can be very intensive as it commonly requires the study of a lot of samples. Microfluidics can drastically reduce the amount of work for conducting experiments, since it allows for multiple samples, independent droplets, to be studied in a short time.

In this study, a previously designed microfluidic setup is used to study two aspects of Non-Photochemical Laser-Induced Nucleation. First, the influence of time on the nucleation process is investigated by increasing the droplet pathway in an improved version of the microfluidic setup, via a longer capillary and a FEP tube coil. Second, the nanoparticle heating mechanism is explored by filtration of a supersaturated KCl solution and doping of a filtered supersaturated solution with iron oxide nanoparticles. Control cooling and laser irradiation experiments are conducted with these solutions to study the effect of nanoparticles on Non-Photochemical Laser-Induced Nucleation.

Results show that increasing the droplet pathway is not that simple because of a coating issue of the capillary that can possibly be solved by trial and error and the formation of dead zones and back flow in the FEP tube coil. The effect of time on the nucleation probability in Non-Photochemical Laser-Induced Nucleation has therefore not been studied up to a satisfying result. Removal of nanoimpurities from a supersaturated KCl soltuion upon filtration gives a significantly lower nucleation probability compared to an unfiltered solution. Addition of iron oxide nanoparticles on the other

hand increases the nucleation probability to 100%. These results highly support the nanoparticle heating model.

Acknowledgements

The 7 months I was working on my thesis have been an absolute pleasure. I gained much experience that goes further than conducting experiments in the lab and it gave me the opportunity to meet many people. Starting from my interest on the field of crystallization, I got the chance to learn much about crystallization and especially NPLIN. There were a lot of challenges during this thesis and without perseverance and the support from others it would not have been the achievement it is now. Therefore I would like to express my gratitude to all the people that supported me during my thesis.

First of all, I would like to thank Dhr. H.B. Eral for providing me with the opportunity of doing this project in the NPLIN group at the Process & Energy (P&E) department of the TU Delft. His suggestions, feedback and comments on my experiments were really supportive and guided me throughout this project. My gratitude further goes out to other members of Eral lab and especially the NPLIN group, who supported me during the many group meetings. A special acknowledgement goes to my daily supervisor Vikram Korede for being available on a daily basis and pushing me towards my limits. Furthermore I would like to thank the lab technicians and the people from DEMO for always making time for me whenever I asked them for help.

Finally I want to thank my parents and friends for their support and showing their interest in my project. Without them, this project would have been a lot more challenging for me.

I hope that you enjoy reading my thesis as much as I enjoyed myself throughtout these 7 months.

Thomas Dubbelman

Contents

List of Figures

1

Introduction

1.1 Introduction

Crystallization is disputably one of the most important and most used separation and purification techniques applied in major industries such as pharmaceuticals, agriculture, fine chemicals and more. Crystallization has two main features: nucleation and growth. Over the years, a lot of successful research has been done in understanding nucleation mechanisms. However, other aspects of nucleation are not yet fully understood. This makes it difficult to design and scale up crystallization processes on an industrial level.

In an effort to gain more control over nucleation and crystal properties, advanced crystallization methods are getting more popular as compared to conventional crystallization methods. One of these advanced crystallization methods that shows a lot of promise is Non-Photochemical Laser-Induced Nucleation (NPLIN). In this technique, a nanosecond laser pulse is shot at a supersaturated solution to trigger instantaneous nucleation, where it otherwise would take several weeks for the solution to crystallize, if no external influences are applied [8]. NPLIN is termed a non-photochemical process because the solution does not absorb any of the laser light when a laser pulse is shot and therefore a photochemical reaction does not take place inside the solution [8].

A great many of studies have been conducted on NPLIN in order to get data on important parameters influencing NPLIN, such as laser intensity, wavelength, laser polarization, supersaturation and impurities. Many

compounds have successfully been crystallized. From the observations made in these experiments, three mechanisms were hypothised in order to explain NPLIN. The first one is based on the Optical Kerr Effect. Here, the electric field of a laser creates a dipole moment such that molecules in the solution align wiht the electric field. This facilitates the structural formation of clusters in the solution and hence the formation of crystals [8]. A second mechanism was proposed by Alexander et al., suggesting that NPLIN might be explained through the Isotropic Electronic Polarization (IEP). Accordign to this explanation, the free energy of a dielectric particle decreases when the particle is submerged in a medium with a lower electric permittivity, this in the presence of an applied optical electric field. The reduction in the free energy leads to a smaller critical nuclei size which improves nucleation kinetics as crystals form earlier than they would normally do. The drawback of this model is that it is unable to explain why NPLIN gives a preference to the formation of certain crystal polymorphs. The third mechanism that is used to explain NPLIN is based on the heating of nanoparticle impurities that are present in a supersaturated solution. The impurities can be naturally present in the solution or pollutes that enter the solution from outside, such as dust particles. It is hypothesized that the nanoparticles absorb part of the incoming laser light and heat up. Thereafter the heat is transfered to the surrounding solution and part of the solvent is vaporized. The vapor bubbles that are created facilitate the aggregation and accumulation of solute molecules at the vapor-liquid interface. This leads to nucleation of the particles and therefore the formation of crystals. Till now, there is no agreement on the mechanisms, as they all fail to explain all of the observations and reported results in experiments.

1.2 Research objectives

The main research objective of this thesis is 'Estimating nucleation kinetics in a microfluidic setup with and without laser exposure'. This objective will be explored in two important aspects. The first aspect to investigate is the influence of residence time on nucleation probabilities in a microfluidic setup, both with and without laser. The study tries to provide an answer to the following question: 'Can the residence time of droplets within a microfluidic setup be increased, and if so, how does it affect the nucleation

probability of the droplets?'. For this thesis a microfluidic setup is used that is developed by a former master student and further improved by another master student to study the effect of NPLIN parameters [6, 28]. In the existing microfluidic setup, droplets currently have a residence time of 70 seconds. This is the time that is required to film the droplets at a single point within the setup. If the residence time is increased, it is hypothesized that a higher nucleation probability can be observed near the end of the setup. Additionally, an extended residence time can allow for one or more extra cameras to be incorporated within the setup. The use of multiple cameras in the microfluidic setup allows for a more thorough analysis of nucleation probability with respect to time. Such data is valuable for estimating nucleation kinetics.

The second aspect has a focus on the influence of impurities on the nucleation probability during laser irradiation experiments. Supersaturated salt solutions naturally contain impurities, which can potentially trigger nucleation. According to the nanoparticle heating model (see 2.2.3), these impurities may have additional effects on nucleation in NPLIN. This study will explore the question: 'Does the nucleation probability in a supersaturated KCl solution change by the addition or removal of impurities under the exposure of a laser?'

1.3 Thesis outline

This thesis report starts with a literature review in Chapter **??**. This literature review provides a broad overview of crystallization and various nucleation models. The discovery of NPLIN is described and an examination of the developments in the field of NPLIN is given. Chapter 2 concludes with a discussion on the role of microfluidics in crystallization. Chapter 3 appoints the challenge of increasing the residence time within the microfluidic setup. Two methods of increasing the residence time are presented, together with their difficulties and limitations. Chapter 4 explores the influence of the removal of impurities in supersaturated KCl solutions on NPLIN. This chapter discusses experiments that involve both control cooling and laser irradiation experiments using KCl solutions that are filtered through filters with various pore sizes. The expectations and outcomes of the experiments are discussed in detail. Building on this,

Chapter 5 looks into the effects of impurity addition, nanoparticles in specific, on the nucleation process. It includes the results of control cooling and laser irradiation experiments using supersaturated KCl-nanoparticle solutions. In the final chapter, Chapter 6, the results from Chapters 3, 4 and 5 are summarized and a conclusion is drawn from the results. Chapter 6 also provides recommendations on future research possibilities based on the findings of this thesis as well as an assessment of the applicability of microfluidics in NPLIN. The thesis concludes with supplementary data provided in the appendices.

2

Literature review

This chapter starts with a general description of crystallization. Then, various factors that influence the nucleation probability are listed as well as nucleation models. Thereafter, the NPLIN phenomena is described in detail together with NPLIN affecting factors. Models that describe NPLIN are presented, with a focus on the nanoparticle heating model. Finally, this chapter finishes with an overview of studies done on the influence of impurities in NPLIN.

2.1 Crystallization

Crystallization is an important separation and purification step in chemical industry. It relies on a phase separation of a solid compound (solute) that is dissolved in a liquid (solvent). This phase separation consists of two steps: nucleation and growth. The driving force of both is supersaturation. When a number of solute molecules group together, they form a cluster. Once the cluster size exceeds a critical radius, the cluster starts to grow and forms a crystal. From a thermodynamic point of view, it is energetically favorable for a cluster at the critical radius to get out of solution. The chemical potential of the solute molecules is then lower compared to solute molecules in the solution. Immediately after nucleation, the crystal grows by the addition of other solute molecules present in the solution. Most crystal properties, such as the morphology and the shape of the crystal, are fully dependent on nucleation. This means that a better understanding of the nucleation process will lead to more control over the crystallization process.

2.1.1 Nucleation mechanisms

In crystallization, there are two known nucleation mechanisms, namely primary nucleation and secondary nucleation. Primary nucleation takes place in a supersaturated single phase system and can further be divided in homogeneous primary nucleation and heterogeneous primary nucleation. In homogeneous primary nucleation, crystals form inside a bulk solution without the help of any foreign bodies. The crystals that are produced therefore only involve solute molecules. In heterogeneous primary nucleation, clusters form at the surface of impurities such as the wall of the crystallizer, dust particles or other pollutes. In addition to primary nucleation, secondary nucleation can take place. Here, a supersaturated solution is seeded with crystals that subsequently initiate nucleation inside the solution. More than primary nucleation, secondary nucleation greatly determines crystal parameters.

As mentioned in 2.1, the driving force behind nucleation and growth is supersaturation, which is derived from a chemical potential difference between a solute molecule present in the solution and a solute molecule in a crystal [27]. For a compound i in a binary (2 species) solution, the difference in supersaturation can be written as

$$\Delta\mu_i = \mu_{i,solid} - \mu_{i,liquid} \tag{2.1}$$

When $\Delta\mu < 0$, nucleation takes place. The chemical potential of a species i is a function of the temperature, a standard chemical potential of that species, the gas constant and the activity of i:

$$\mu_i = \mu_i^0 + RT \ln a_i \tag{2.2}$$

Combining equations 2.1 and 2.2 leads to the following:

$$\Delta\mu_i = RT \ln \frac{a_i}{a_i^*} = RT \ln S_i \tag{2.3}$$

In equation 2.3, a_i^* is the activity of a supersaturated solution and S is the supersaturation ratio. The supersaturation ratio can be expressed in terms of concentrations:

$$S_i = \frac{c_i}{c_i^*(T)} \tag{2.4}$$

c_i is the concentration of solute i in the solution and c_i^* is the equilibrium concentration of solute i at a defined temperature. c_i^* does also depend on the nature of both the solute and the solvent. A solution with S > 1 is called a supersaturated solution and a solution with S < 1 is called an undersaturated solution. The equilibrium concentration goes up with temperature, meaning that at a higher temperature a larger quantity of solute i can be dissolved. This can be shown with for example a solubility curve (see Figure 2.1).

At a temperature T_2, a solute has an equilibrium concentration C_2 inside a solution. This point is on the solubility line and is indicated with **a**. At point **a**, the solution has a supersaturation of S = 1. If the solution cools down, the supersaturation of the solution increases as the equilibrium concentration is lower at a lower temperature. It is then in the metastable

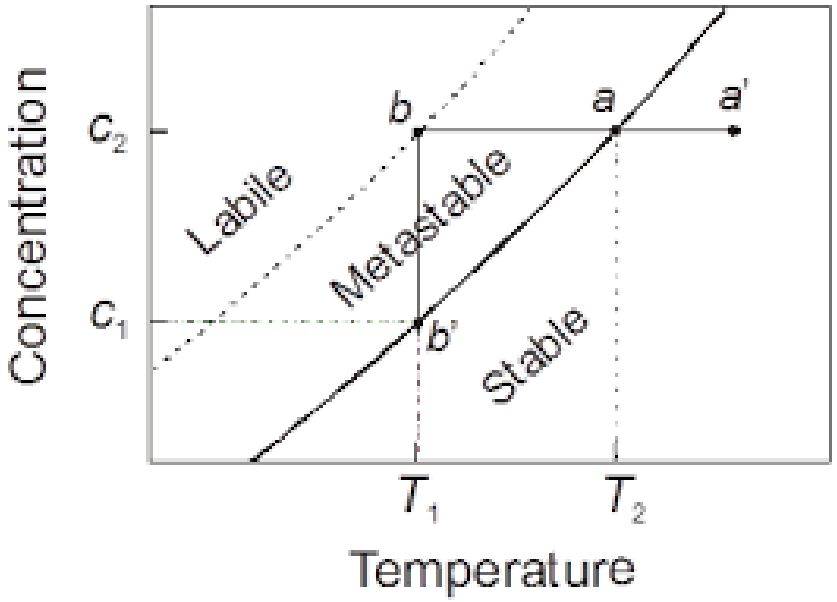

Figure 2.1: Solubility curve (thick line) with and metastable zone limit (dotted line). Image obtained from literature [23].

zone where the solution can nucleate, but not spontaneously. When the solution is cooled to temperature T_1, point **a** is shifted to point **b** on the metastable zone limit. At this point or any other point in the labile zone, the solution is not stable anymore and starts to crystallize. The concentration then goes from c_2 to c_1, which is the equilibrium concentration at T_1.

Currently, there are two mechanisms that explain how a nuclei is formed. These are the classical nucleation theory (CNT) and the two-step nucleation theory (TSN).

2.1.2 Classical nucleation theory

One of the oldest theories to describe nucleation is the classical nucleation theory (CNT). The theory is based on the work of Gibbs (classical thermodynamics) [27] and further developed by others [13]. The theory is able to describe the nucleation probability based on a number of variables. These variables include supersaturation, temperature, dielectric properties of the solute, laser wavelength, and laser intensity [26]. The classical nucleation theory starts with the nucleation rate J, given by 2.5 [3].

$$J = J_0 D Z \exp \frac{-W^*}{k_B T} \tag{2.5}$$

In this equation, J_0 is a pre-exponential factor, D is the diffusion coefficient, Z is the Zeldovich factor, W^* is the nucleation work, k_B is the Boltzmann constant and T is the temperature. The nucleation work can be derived from the free energy W as a function of the nucleus size. The free energy is equal to the sum of the Gibbs free energy of cluster formation ΔG_v and the Gibbs free energy of surface creation ΔG_s. ΔG_v can be expressed as:

$$\Delta G_v = v \rho \Delta \mu \tag{2.6}$$

In this equation, v is the volume of a nucleus and ρ is the number of molecules in a cluster. Expressing equation 2.3 on a molecule basis and substituting it in equation 2.6 leads to the following:

$$\Delta G_v = v \rho k_B T \ln S \tag{2.7}$$

An expression for ΔG_s is given by equation 2.8:

$$\Delta G_s = cv^{\frac{2}{3}} n^{\frac{2}{3}} \gamma \tag{2.8}$$

In this equation, v is the molecular volume of a single crystal and γ is the surface energy at the boundary of the nucleus with the solvent. The free energy is then expressed as:

$$W(n) = v\rho k_B T \ln S + cv^{\frac{2}{3}} n^{\frac{2}{3}} \gamma \tag{2.9}$$

The nucleation work is the maximum free energy which is found at the critical nucleus size. From equation 2.9, equation 2.10 can be derived to describe the nucleation work:

$$W^* = \frac{16\pi\gamma^3 v^2}{3k_B^2 T^2 \ln S^2} \tag{2.10}$$

Substitution of equation 2.10 in equation 2.5 gives a final expression for the nucleation rate where A is a pre-exponential factor containing J_0, D and Z:

$$J = A \exp -\frac{16\pi\gamma^3 v^2}{3k_B^3 T^3 \ln S^2} \tag{2.11}$$

The classical nucleation theory is the most used theory to describe nucleation. However, it often fails at providing an explanation for observations from experiments. This is due to a number of assumptions that are made. These include:

- Nuclei are considered to be spherical and isotropic
- Crystals growth in a step-like manner
- Surface energies are independent of temperature, size and curvature

- Nucleation is independent on time
- Formation of nuclei does not affect the vapor phase

Due to limitations in the classical nucleation theory, the two-step nucleation theory has gained more interest.

2.1.3 Two-step nucleation theory

The two-step nucleation (TSN) theory describes nucleation with a mechanism involving two steps. According to the TSN theory, a metastable phase exists inside a supersaturated solution that has a stability that is between that of the considered crystal phase and that of the solution. The metastable phase then undergoes a phase transition to the nearest stable state [16, 17]. The difference between the classical nucleation theory and the two step nucleation theory is shown in Figure 2.2. In the first step of TSN, solute molecules agglomerate to form a high-density area inside the solution. Subsequently in the second step, when the agglomerates in this area reach a critical nucleus size, the solute molecules form an ordered structure and a crystal is formed [27]. Besides the crystal size, which is the single parameter used in the classical nucleation theory, the two-step nucleation theory also uses crystallinity as a parameter. The two-step nucleation model has been used to describe non-photochemical laser-induced nucleation. Garetz et al. suggested that an electrical field can induce alignment of molecules inside a solution which facilitates the ordering of solute molecules to form a crystal [8].

2.2 NPLIN

NPLIN (short for non-photochemical laser induced nucleation) was first discovered by accident in 1996 [8]. In a study on second harmonic generation in supersaturated urea solutions in water, it was noticed that laser pulses can induce nucleation in the solution. The wavelength of the laser was near infrared, a photo-chemical mechanism was ruled out as an explanation of the phenomena. Initially, an electric-field-induced effect was suggested to explain the phenomena, leading to the optical Kerr effect (OKE) (see Figure 2.2.1). The phenomena was named nonphotochemical laser-induced nucleation (NPLIN). Later, other nucleation mechanisms for

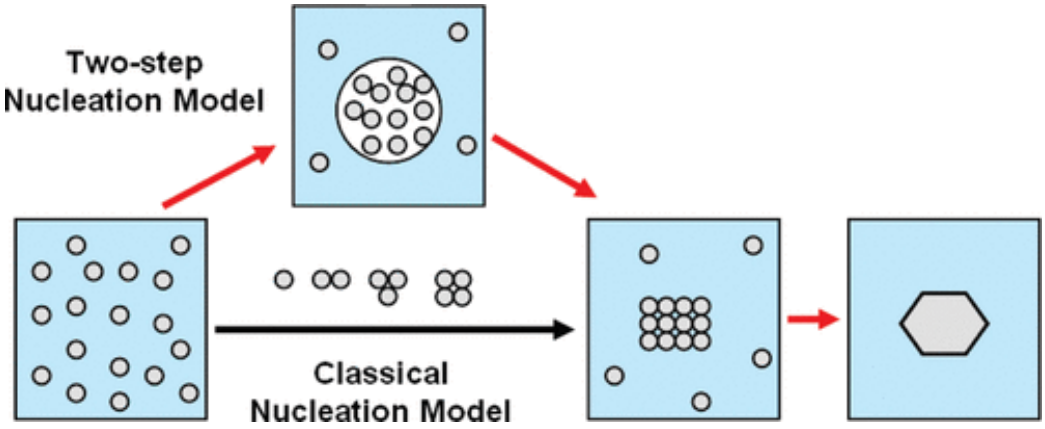

Figure 2.2: CNT vs STD. Image obtained from literature [7].

NPLIN have been proposed (see 2.2). Soon after the first encounter with NPLIN, experiments have been done with NPLIN and glicine solutions. In one of the first of those experiments it was showed that the polarisation of the laser can change the morphology of the crystals formed [31]. Because of increasing interest in the research of Garetz et al., more experiments towards laser parameters and solution properties were performed. These included the time of the laser pulse shot, the effect of supersaturation, the species of solute and parameters such as laser intensity and wavelength [2].

2.2.1 Optical Kerr Effect

Certain liquid transparent samples, such as salt solutions, can change the direction of an incident light beam under the presence of an electric field [25]. This phenomena is called the Optical Kerr Effect (OKE). In a supersaturated solution, there is a continuous formation and separation of nuclei. According to the Optical Kerr Effect, this means that when a laser passes through a supersaturated salt solution, the solute molecules in the solution will align with the laser. The chance that the critical radius is exceeded and nucleation takes place is then higher. However, at the applied laser intensity the electrical field is not strong enough to align molecules. Other models are proposed and further developed to describe NPLIN [2].

2.2.2 Dielectric polarization model

The Optical Kerr model fails to describe NPLIN. Therefore a second mechanism that is used to explain NPLIN is the dielectric polarization (DP) model. This mechanism was first proposed by Alexander et al. and is according to the classical nucleation theory (CNT) [1]. At the wavelength of the laser used in NPLIN experiments, the laser energy is not adsorbed by either the solid or the solvent. The electrical field of the laser therefore is able to polarize the electrons in the solute atoms, lowering the free energy of the clusters. As in classical electromagnetism, the precritical solid cluster acts as a dielectric body and the solvent as a dielectric continuum [2]. The free energy of the clusters is calculated with the formula:

$$\Delta G = -v(\epsilon_p - \epsilon_s)E^2 \tag{2.12}$$

In this equation, v is the volume of cluster, ϵ_p is the permittivity of the cluster and ϵ_s is the permittivity of the solution. Because, the permittivity of the precritical solid cluster, ϵ_p is higher than the permittivity of the solvent surrounding the cluster, ϵ_s, the electrical field stabilizes the cluster with respect to the solution. The critical size of the clusters then becomes smaller, facilitating nucleation. An important assumption in the dielectric polarization model is that the precritical cluster is presented as a sphere. The dielectric polarization model has proven to be a good fit for experimental data from NPLIN experiments. It can therefore be used to describe the nucleation probability, $P_{nucleation}$, with the following functions:

$$N_{crystal} = mI \tag{2.13}$$

$$p_{nucleation} = 1 - \exp -mI \tag{2.14}$$

$$m = \frac{3N_{molecule}\gamma\alpha}{2\pi\rho^3(k_BT\ln S)^2} \times \frac{\exp -\Delta G_{c(0)}/k_BT}{\int_0^{r_c(0)} r^3 \exp -\Delta G_{(r,0)}/k_BT dr} \tag{2.15}$$

In these equations, $N_{crystal}$ is the average number of crystals that are produced, m is a liability constant that reflects the susceptibility of the solution to nucleation upon radiation and I is the laser intensity.

2.2.3 Nanoparticle heating model

Both the OKE and DP mechanisms can't describe all observations in NPLIN experiments. These models are not able to explain why there is a laser threshold intensity and why some systems are not susceptible to NPLIN at all. It has been shown that upon filtration of a supersaturated solution, the nucleation probability goes down in NPLIN experiments [2]. This suggests that the solution contains very small impurities that interact with the laser. In addition, NPLIN experiments have been done with carbon dioxide gas as the nucleated phase [18]. These experiments showed that the permittivity of the carbon dioxide was lower than the permittivity of the solution. This is clearly not according to the DP model (see 2.2.2) and the OKE model. Therefore a third mechanism is proposed, called the nanoparticle heating (NP) model. In this model, a nanoparticle is heated by the laser pulse, where after the fluid surrounding the nanoparticle evaporates. It is suggested that at the interface of the vapor bubbles with the solution, it is more difficult for the solute to stay in a dissolved state. The solute might therefore cluster and nucleate. Also, the vapor bubble surrounding the nanoparticle can collapse, inducing nucleation. As a result of laser heating and the vapor bubble collapsing, the nanoparticle might break, creating new interfaces for nucleation (see Figure 2.3). So unlike the OKE and DP models, the nanoparticle heating model is based on nanoparticle impurities rather than an electric field affecting solute clusters.

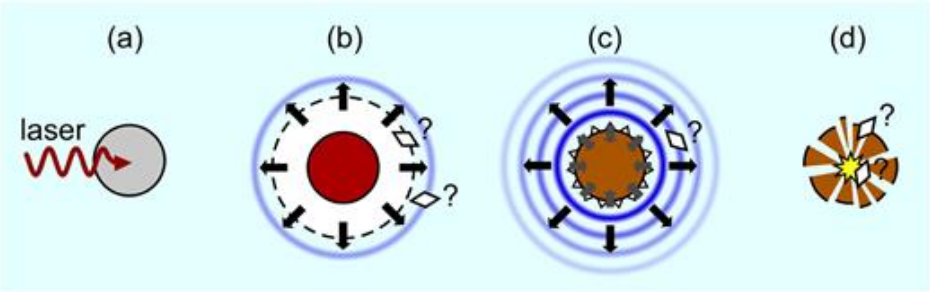

Figure 2.3: A possible scenario for the nanoparticle heating model. (a) The nanoparticle absorbs energy from the laser. (b) Fluid surrounding the nanoparticle evaporates, creating local high supersaturation. This might induce nucleation. (c) The vapor bubbles collapses which can cause nucleation. (d) The nanoparticle breaks because of laser heating and the vapor bubble collapsing, creating interfaces for nucleation. Image obtained from literature [2].

If solid impurities really are the cause of NPLIN as is explained by the nanoparticle heating model, the evident questions are then - what is the nature of these impurities and where do they come from? Ward et al. filtered large amounts of a nearly supersaturated (s = 0.95) ammonia solution through a membrane of 0.2 μ m and analysed the residue on the filter. They found that the impurities had a size below the mircon scale and mainly consisted of iron and phosphate [30]. These impurities were found to be specific to the manufacturer's ammonia. This means that other solutions might contain different impurities. Ward et al. also studied the effect nanoparticles by conducting NPLIN experiments with supersaturated ammonia solutions doped with iron oxide nanoparticles. Results show that the doped solutions have a higher nucleation probability than filtered solutions, but similar to unfiltered solutions.

The nanoparticle heating model provides a better explanation for observations from NPLIN experiments than both the OKE model and the DP model. However, there is the possibility of multiple effects into play. [2]. Therefore the reproducibility of NPLIN experiments might depend on the type of impurities present inside the solution.

3

Longer residence times

The nucleation probability of a supersatured solution is valuable information for estimating nucleation kinetics. A microfluidic setup is used to gain nucleation probabilities by analyzing a lot of samples, about 1000 droplets. Each of these droplets acts as an independent crystallizer reactor, meaning that the droplets don't have any interaction with each other. A schematic picture of the microfluidic setup is given in Figure 3.1. The microfluidic setup constists of three important sections: the droplet generation zone, the laser exposure zone and the crystal observation zone.

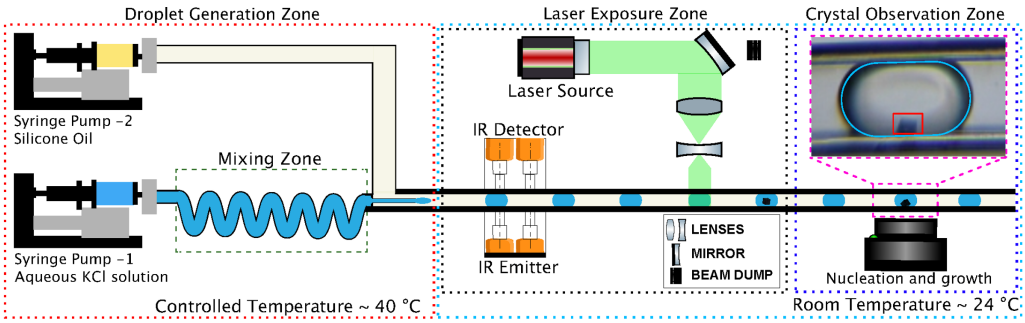

Figure 3.1: A schematic drawing of the microfluidic setup.

The droplet generation zone has an environment that is kept at 40 °C. The temperature of 40 °C ensures that there is no unwanted nucleation in this part of the microfluidic setup as the droplets are generated. In the droplet generation zone there are two microfluidic pumps (NE-1002X-ES,

New Era Pump Systems Inc.) that each can hold a syringe. One of the microfluidic pumps is used to generate a continuous phase (silicone oil) and the other pump is used to generate a dispersed phase (KCl solution). The flowrate of the dispersed phase is set at 10 μL/min, while the flowrate of the continous phase is set at 100 μL/min. Both microfluidic pumps are connected to a PTFE tube (900 μm diameter). Right after the dispersed phase leaves the pump, it enters a mixing zone made with bends. The bends assure that there is ideal mixing of the solution in a form of passive mixing. After leaving the mixing zone, the dispersed phase joins the continuous phase via a T-junction. The dispersed phase then flow around an inner capillary (VitroCom Inc., borosilicate, 700 μm diameter) that is surrounded by a square capillary (VitroCom Inc., borosilicate, 900 μm side) where the continous phase flows through. The end of the inner capillary is tapered such that the dispersed phase forms droplets when passing the inner capillary. In order to prevent the droplets from sticking to the capillary walls, the capillary is coated .

When the droplets leave the droplet generation zone, they enter the laser exposure zone. Because the droplets are not in the 40 °C enviroment anymore, they start cooling down to the room temperature of 25 °C. Because the droplets are cooling down, they get supersaturated before they are irradiated with the laser. At a distance of 8 cm after the temperature-controlled environment, droplets are irradiated with an unfocused pulsed laser beam ((10 Hz, 9 mm diameter, Nd-YAG laser, Continuum Powerlite DLS 8000). With 2 lenses and a mirror (see Figure 3.1), the laser is directed to the capillary such that the desired laser intensity and beam diameter are reached.

16 cm after the point where the droplets are hit by a laser the crystal observation zone is located. When travelling to the crystal observation zone, droplets have time to undergo nucleation and crystals might form inside the droplets. Droplets that flow through the capillary are filmed with an objective lens (4X, 0.1 NA), a microscopic camera, and a diffuse white LED. The time that a droplet travels from the point where the laser hits the capillary to the point where the camera is placed is approximately 70 seconds. The number of droplets that pass the camera are manually counted from the video of the passing droplets. Also, the number of droplets with one or more crystals is manually counted from the video. These two numbers

are used to calculate the nucleation probability.

3.1 Flow rate, droplet speed and residence time

In the current microfluidic setup the residence time is 70 seconds. This represents the duration of a droplet remaining in the 30 cm capillary. As the residence time goes up, the nucleation probability is expected to increase as well, because the droplets then have more time to cool down at a defined supersaturation. To empirically determine nucleation probabilities at higher increased residence times, it is essential to explore methods for extending the residence time within the microfluidic setup. There are two adjustable parameters that can facilitate this: the flow rate of both the continuous and dispersed phase and the droplet pathway length. The first approach involves the reduction of the flow rate of the continuous and dispersed phase. This corresponds to an increase in the residence time. The second approach involves increasing the droplet pathway, which would also result in longer residence times. The relationship between residence time, flow rate and droplet pathway is:

$$t = l * A/Q_{tot} \tag{3.1}$$

Here, t is the residence time, l is the distance covered by the droplet through the capillary, A the surface and Q_{tot} is the combined flow rate of the continuous and dispersed phase. Decreasing the total flow rate could potentially disrupt the droplet flow, making it a less favorable approach. Therefore the most effective strategy to increase the residence time is likely to be increasing the length of the droplet pathway. In section 3.2, a microfluidic setup that incorporates a 60 cm capillary is investigated. Subsequently, in paragraph 3.3, a microfluidic setup equiped with a Fluorinated Ethylene Propylene (FEP) tube coil is examined.

3.2 60 cm capillaries

By increasing the length of the capillary used in the microfluidic setup, a longer residence time can be obtained. Instead of the normally used 30 cm capillary, a 60 cm capillary with the same diameter is used in an improved

microfluidic setup (see Figure 3.2). Compared to the microfluidic setup described in the beginning of the chapter, this one has an extended crystal observation zone with a second objective lens, a microscopic camera and a diffuse white LED. At the same flow rates, the residence time of the droplets inside the setup is now doubled, from 70 seconds to 140 seconds. This means that a higher nucleation probability is measured at the end of the capillary.

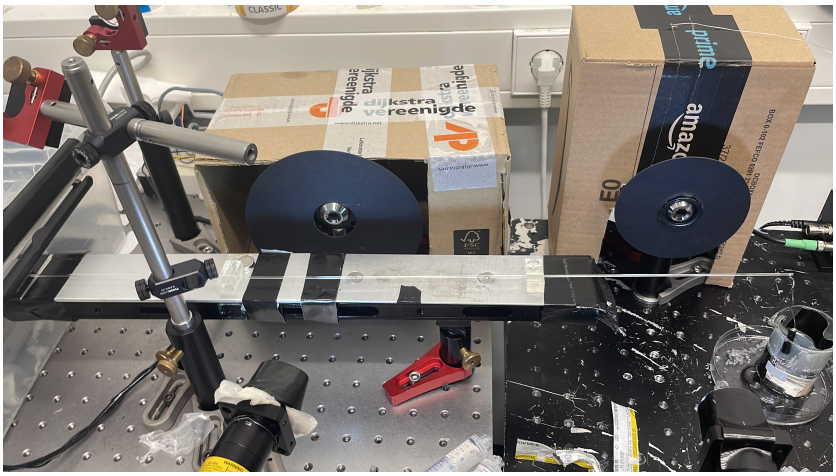

Figure 3.2: Improved microfluidic setup.

To coat a 60 cm capillary, the procedure for 30 cm capillaries is adopted with slight modifications (see A.2). Because of the absence of a suitable desiccator for the 60 cm capillaries, a custom-built desiccator is used (see A.3). Cooling and laser control experiments are conducted by using the 60 cm capillaries and a 1.10 supersaturated KCl solution (see B.1). This facilitates a direct comparison with the results from a 30 cm capillary and a KCl solution with the same supersaturation. During these experiments, clogging is observed at a point in the capillary between the first and the second camera, indicating a potential compromise of the nucleation probability. Several factors are considered that can potentially cause this clogging. Firstly, the inner capillary is fragile. It might break upon insertion during the experiment. After repeating the experiment multiple times, the inner capillary is ruled out as a possible cause due to the negligible probability of consequent

breakage of the inner capillary. Secondly, the temperature inside the temperature controlled environment is investigated. The temperature inside the controlled environment is maintained at 40 °C such that sudden and gradual decreases in the temperature can cause nucleation inside the bulk solution and the capillary, leading to clogging. However, the temperature in the controlled environment is constantly monitored while conducting the experiments. Therefore this temperature is eliminated as a possible cause. Finally, the ambient room temperature is examined. If the temperature around a part of the capillary drops below 25 °C, clogging can occur at that specific location. To verify that the temperature around the capillary is indeed 25 °C or higher, temperature measurements are conducted at five points along the capillary by using a thermocouple. Each measurement is repeated 3 times, with and without heating of the hairdryer. Regardless of wether the hairdryer is turned on or off, temperature measurements show that the temperature around the entire capillary is above 25 °C. Thus, it is concluded that clogging is not a temperature related problem. After examining all factors, the coating of the capillary comes up as the remaining variable. Despite numerous attempts, successfully coating a 60 cm capillary proves to be challenge. A properly coated 60 cm capillary might be achieved via a process of trial and error. Given the time constraints of this project, the decision is made to explore an alternative method for increasing the residence time.

3.3 FEP tube coil

Attempts of using 60 cm capillaries to increase the residence time have proven to be problematic because of coating issues. A pre-coated FEP tube can possibly replace the 60 cm capillary. By adjusting the length of the FEP tube, we can control the residence time in control cooling and laser irradiation experiments. A piece of FEP tube, corresponding to a residence time of approximately 7 minutes, is coiled around a metal bar and installed in the microfluidic setup (see Figure 3.3). Ideally the FEP coil should be connected directly to the mixing zone. However, such a direct connection to the mixing zone is not feasible and will likely result in leakages. Therefore a 30 cm capillary, that is connected to the mixing zone, is attached to the coil. The inner diameter of the FEP coil is made equal to the outer diameter of the capillary such that the flow velocity remains

roughly consistent. The total flow rate that is used in conventional cooling control and laser irradiation experiments is 110 µm/s. However, this flow rate is not high enough for proper flow through the coil due to a height difference that the flow has to overcome. Therefore, the total flow rate is doubled to 220 µm/s.

Figure 3.3: FEP tube coil in the microfluidic setup.

Although the transition from the capillary to the FEP tube is a good fit, it presents some concerns. This is primarily because of the geometry change from a square capillary to a round tube. This geometry change may lead to variations in flow and droplet shape, thus potentially causing unwanted nucleation. Initially, when conducting control cooling experiments with the FEP tube and a KCl solution at a supersaturation of 1.10, the geometry change does not seem to be of any concern regarding the geometry change. Droplets reach the end of the coil and show minimal deformation upon entering the tube. However, during the cooling experiments, the flow through the coil appears to be slower than through the capillary. At the junction between the capillary and the FEP tube, a leakage seems to occur, due to the fit not being tight enough which leads to deformation of the tube. The leakage leads to a reduction in the coil flow due to backflow.

Additionally, there are 'dead spaces' that form at the transition point, where the continuous and dispersed phase are not flowing at all, creating potential hotspots for unwanted nucleation [21]. Both the leakage and the formation of 'dead spaces' can not be eliminated in a way that allows the reuse of the FEP coil. During the term of the project, a resolution for these problems has not been found. Consequently, due to time restraints, the exploration of implementing a FEP coil is discontinued, as is the investigation into performing experiments with increased residence times.

4

Filter experiments

4.1 Filtration of solution

The NH model tries to attribute the nucleation in laser irradiation experiments to nano-sized impurities. The nature of the impurities and their size are yet unknown. To verify whether impurities do play a role in NPLIN and thus laser irradiation experiments, filtered KCl solutions are used in microfluidic crystallization experiments instead of unfiltered KCl solutions. Because the size of the impurites is unknown, filters with different pore sizes are used. The nulceation probabilities obtained with 3 different filtered solutions in control cooling and laser irradiation experiments are compared to the nucleation probability of an unfiltered KCl solution.

4.1.1 Results

To investigate the influence of filtration on NPLIN probability, a series of experiments are conducted with a KCl solution (S = 1.10) with filters of different pore size, namely 0.22 μm (PTFE syringe filter), 0.45 μm syringe filter (PTFE syringe filter) and 7 μm paper filter (Grade-3HW, Whatman filter) (see B.2). The experiments are carried out by using the developed microfluidic setup and include both control cooling experiments and laser irradiation experiments with an incident wavelength of 532 nm and a peak intensity of 50 MW/cm^2. The nucleation probabilities that are obtained in these experiments are shown in Figure 4.1 (A).

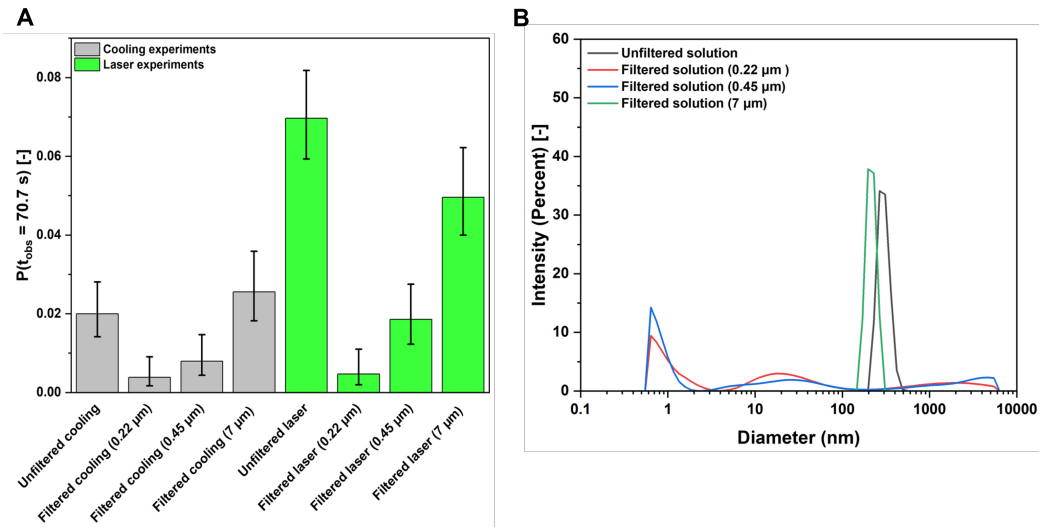

Figure 4.1: (A) Nucleation probabilities for filtered solution with different pore size diameters and unfiltered solution under S = 1.1 in both control cooling & laser experiments at a constant laser wavelength (532 nm) and constant theoretical peak intensity (50 MW/cm^2) and (B) Particle size distribution obtained for unfiltered KCl solution and filtered KCl solution with 0.22 μm, 0.45 μm and 7 μm filters.

A higher nucleation probability is observed in laser experiments with an unfiltered solution as compared to a filtered solution with 0.22 μm and 0.45 μm pore size filters. Moreover, laser irradiation increases the nucleation probability in the unfiltered solution, while for the filtered solution no significant difference is seen between control cooling and laser irradiation experiments for 0.22 μm and 0.45 μm pore size filters. This observation is ascribed to the presence and absence of impurities in the unfiltered and filtered solutions, respectively, which are intrinsically related to the (nano)impurity heating mechanism that is proposed for the NPLIN phenomena [18, 12, 14]. Yet another explanation for the observed reduction in the nucleation probability upon filtration is the reduction of existing KCl clusters due to the high shear force produced as the fluid travels through the sub-micrometer size pores of the filter. As drag force scales with size at low Reynolds number flows [9], disordered clusters that are discussed in two-state nucleation theory [7] may be broken into smaller sizes or dissolve back into the solution upon filtration. Further laser experiment results show a similar nucleation probability for both the 7 μm pore size filtered solution and the unfiltered solution. This indicates that the 7

μm filter is ineffective in removing nanoimpurities/nanoclusters present in the solution. This is further supported by the similar results obtained for control cooling experiments. These findings suggest that the initial presence of nanoimpurities/nanoclusters in the unfiltered solution might be larger than 0.45 μm in mean hydrodynamic diameter and could not be effectively filtered by the 7 μm pore size filter. A supportive evidence to this claim also comes from Dynamic light scattering (DLS) data for these experiments as shown in the Figure 4.1 (B).

Dynamic light scattering (DLS) is used to estimate the particle size distributions in KCl solutions. To prevent spontaneous nucleation, the KCl solution is slightly undersaturated (S = 0.98). The non-negative least squares approach is used to compute the particle size distribution from the DLS data. The measurements are performed for an unfiltered KCl solution and filtered KCl solutions with different pore size filters (0.2 μm, 0.45 μm, 7 μm). The particle size distribution of the unfiltered solution reveals a mean hydrodynamic diameter of 264 ± 50 nm. Upon filtration with 0.22 μm and 0.45 μm filters, particles at 264 ± 50 nm are eliminated, resulting in a residual population of particles $\leq$ 70 nm and $\leq$ 200 nm, respectively. Still for solutions filtered with 0.22 μm and 0.45 μm filters, peaks are seen in $\leq$ 1 nm. However, literature reports that particle populations $\leq$ 1 nm from DLS measurements were identified as scattering from the solute and do not correspond to a true representation of the particles in solution [30]. In contrast, filtration with a 7 μm filter produced a particle size distribution in a similar size range to that of the unfiltered solution with a mean hydrodynamic diameter of 209 ± 14 nm. These findings suggest the 7 μm filter is not effective in eliminating nanoimpurities or clusters and leads to a nucleation probability comparable to that of the unfiltered solution. Similarly, the 0.22 μm and 0.45 μm filters effectively remove nanoimpurities from the unfiltered solution, thus resulting in lower nucleation probability. The obtained results in Figure 4.1 provide supporting evidence for the nanoparticle heating mechanism [20].

5

Nanoparticles

5.1 Doping with nanoparticles

As we saw in Chapter 4, in laser experiments there is a lower nucleation probability of a supersaturated KCl solution upon filtration, possibly because of impurity removal. This would mean that the higher nucleation probability seen in laser irradiation experiments compared to control cooling experiments [19] is due to the presence of nano-sized impurities. These nano-sized impurities might interact with the laser via a yet unknown mechanism. To determine if there is indeed an effect of nano-impurities on the nucleation probability in laser irradiation experiments, a set of control cooling and laser irradiation experiments is performed with a KCl solution doped with a known amount of nanoparticles. In order to make these solutions, a KCl stock solution (C = 5.42 mol/kg, S = 1.127) is prepared. Subsequently, the solution is filtered in a clean bottle at 50 °C. Because we saw in Chapter 4 that a 0.45 μ m filter is possibly effective in removing impurities, the same filter is used here. Once the solution is filtered, 1.25 g of a nanoparticle suspention is added to the filtered solution. This resulting solution has a concentration of 5.29 mol/kg (S = 1.1) (see B.3). The nanoparticle suspension contains iron oxide nanoparticles (≥97%, CAS: 1317-61-9, 50-100 nm nominal diameter) dispersed in pure water.

There are several properties of the nanoparticle suspension that might have a direct influence on the nucleation probability. These include the nature of the nanoparticles, the size of the nanoparticles, agglomeration, the addition and the amount of surfactant, the sonication time and the amount

of nanoparticle suspension added to the solution. The exact effect of these factors on the nucleation probability is yet unknown. With the exception of the nature of the nanoparticles, the other uncertainties will not be part of my investigation.

The addition of nanoparticles to a KCl solution is expected to increase the nucleation probability in control cooling and laser irradiation experiments. In cooling experiments, the nanoparticles can provide a surface for heterogeneous nucleation [5]. In laser experiments, there can be an added effect of the interaction of nanoparticles with the laser. This is according to the nanoparticle heating model (see 2.2.3).

One of the difficulties of working with a nanoparticle suspension is sedimentation. When a nanoparticle suspension is stored, over time the nanoparticles will sink to the bottom [22]. If such a nanoparticle suspension is added to a KCl solution, the nanoparticles will not be well mixed inside the solution. This means that when droplets of the solution are made in a microfluidic system, the droplets will have varying concentrations of nanoparticles. To make sure that the nanoparticles won't sediment significantly during the time of an experiment, sonication is used. With sonication, ultrasound waves are generated. These waves disperse the nanoparticles in a suspension, such that there is an equal distribution of nanoparticles in the suspension. In the microfluidic system, each droplet formed will then contain a similar amount of nanoparticles. Another difficulty of nanoparticle suspensions is that of agglomeration. Nanoparticles tend to get together inside a suspension, forming clusters of different sizes [10]. This makes it challenging to get control over the size of nanoparticle clusters inside the solution. Sonification is used to counteract agglomeration as well. However, the nanoparticles will still agglomerate a little bit in the suspension and form agglomerates. To determine the size of the agglomerates, dynamic light scattering (DLS) is used (see 4.1.1).

5.1.1 Results

Laser-induced nucleation experiments are conducted with a filtered solution (0.45 μm pore size filter) doped with Fe_3O_4 nanoparticles (50 - 100 nm

nominal diameter) with a concentration of 14.6 μg/ml in solution droplets, with an laser wavelength of 532 nm and a peak intensity of 50 MW/cm^2 to determine whether the addition of nanoparticles can increase the nucleation probability by interaction of the nanoparticles with the laser. The results in Figure 5.1 show a nucleation probability of 100%, with multiple crystals formed in a single droplet, compared to unfiltered and filtered laser experiments where mostly a single crystal per droplet is observed. A possible explanation for the presence of multiple crystals per droplet is the high number of nucleation sites that are active within the droplet in the form of nanoparticles. Another explanation for this phenomenon is the use of multiple laser shots (10-15) per droplet. Multiple laser shots can trigger secondary nucleation events within the droplet. Similarly, control cooling experiments performed with a filtered solution doped with Fe_3O_4 nanoparticles results in a nucleation probability comparable to that of an unfiltered and a filtered solution (0.45 μm pore size filter) in control cooling experiments. These results provide additional support for the observations derived from laser experiments, indicating that the dopant nanoparticles may not be intrinsically enhancing the nucleation process through heterogeneous nucleation. Instead, it is plausible that the interaction of nanoparticles with the laser is the primary contribution to the observed nucleation behavior.

The increase in nucleation probability for KCl-nanoparticle solutions can be ascribed to the fact that Fe_3O_4 nanoparticles exhibit a specific absorption efficiency when exposed to 532 nm laser light that depends on the size of the nanoparticles. This allows for an estimation of the energy absorbed by the nanoparticle from the laser. Quantitative information about specific absorption to size of the Fe_3O_4 nanoparticle can be found in the work from Nagalingam et al. [24]. This energy can further be used to vaporize the surrounding liquid and create a vapor bubble. To calculate the size of the vapor bubble formed from laser irradiation, we can use simple thermodynamic calculations, assuming that one laser shot on one nanoparticle produces a single vapor bubble [29]. However, the DLS result of the filtered doped solution shows a PSD with a mean hydrodynamic diameter of 465 ± 33 nm. This reveals that iron oxide nanoparticles are agglomerated within the supersaturated solution, a problem that is normally encountered in solutions with a high ionic strength [32]. As a

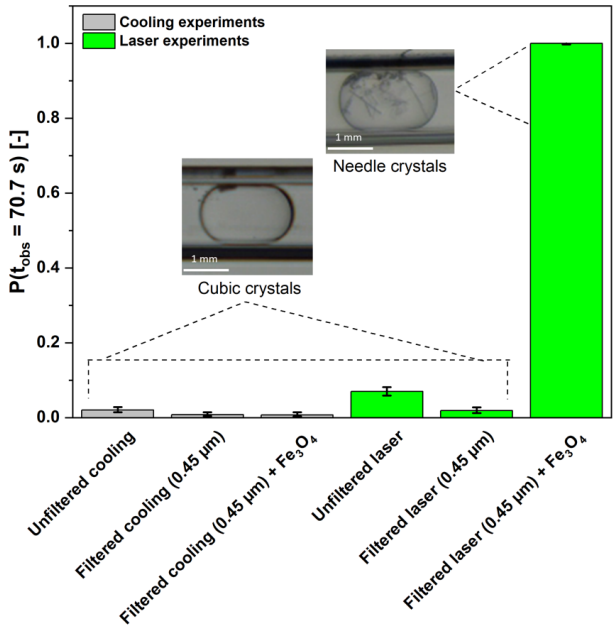

Figure 5.1: Comparison of nucleation probabilities for filtered solution along with addition of Fe_3O_4 nanoparticles and unfiltered solution under S = 1.1 in both control cooling & laser experiments at a constant laser wavelength (532 nm) and constant theoretical peak intensity (50 MW/cm^2).

consequence, treating the agglomerated nanoparticles as a single particle may not be entirely accurate, given that agglomeration leads to modifications in the nanoparticles properties, such as variations in the optical characteristics [32] of the agglomerates. These differences affect the way the agglomerated nanoparticles interact with the laser. An accurate estimation of the bubble size for the agglomerated nanoparticles is beyond the scope of this thesis.

At this stage, it is hypothesized that upon laser irradiation of the filtered doped solution, there might be numerous vapor bubbles that will eventually merge into a larger bubble compared to the bubble size that will be obtained in an unfiltered solution. The maximum size of the bubble, as predicted by Hidman et al. [11] numerically and by Nagalingam et al. [24] combining experiments and numerics, will lead to a higher local supersaturation around the vapor-liquid interface. The increased local supersaturation can accelerate the nucleation process. This explains the much higher

nucleation probabilities that are observed in doped solutions as compared to unfiltered solutions upon laser irradiation. Furthermore, the morphology of crystals within the droplets obtained in laser-irradiated doped solutions, as compared to unfiltered solutions, supports this hypothesis. In every droplet containing nanoparticles, multiple needle-shaped crystals are observed, suggesting that high local supersaturations are produced upon laser irradiation. This is consistent with reports on the tendency for needle-shaped KCl crystals to form in solutions with a high supersaturation. In contrast, the presence of mostly cubic KCl crystals in almost every droplet of laser irradiation experiments with unfiltered solutions indicates relatively lower local supersaturation, aligning with the typical formation of cubic crystals in solutions with a lower supersaturation [15, 4].

6

Conclusion

6.1 Conclusions

6.1.1 Longer residence time

In the first part of this thesis, the influence of residence time on the nucleation probability in microfluidic NPLIN experiments has been studied. Therefor an improved microfluidic setup was used. In this setup, a residence time of 140 seconds was not yet possible. Coating of a 60 cm capillary was problematic as it led to clogging. The protocol for coating a 30 cm capillary has been used as well as slight variations.

Increasing the residence time by connecting a FEP tube coil to a capillary in the microfluidic setup led to back flow, the formation of dead zones and subsequently unwanted nucleation. This was due to an improper fit of the tube caused by the geometry change.It was therefore not possible to extend the residence time in the microfluidic setup with a FEP tube coil.

6.1.2 Filtration and doping of supersaturated solutions with nanoparticles

Control cooling and laser control experiments of supersaturated KCl solutions with filters of different pore size show the possibility of impurity interaction with laser. Upon filtration of the solution with a 0.22 μm filter and a 0.45 μm filter, the nucleation probability lowered significantly from that of an unfiltered solution. However, filtration with a 7 μm filter is ineffective as it gives the same nucleation probability as an unfiltered solution.

In addition, dynamic light scattering revealed that the mean hydraulic diameter of the particle size distributions in the unfiltered solution (264 ± 50 nm) and the 7 μm pore size filtered solution (209 ± 14 nm) are similar. Filtration of the solution with 0.22 μm and 0.45 μm filters completely remove these particles. It can therefore be concluded that either filtration is able to remove impurities with a mean hydraulic diameter larger than 0.45 μm and smaller than 7 μm from the solution or solute clusters form after filtration.

The addition of iron oxide nanoparticles to a supersaturated KCl solution led to a nucleation probability of 100% in laser irradiation experiments, with multiple crystals in a single droplet. Control cooling experiments show a nucleation probability similar to that of an unfiltered and a filtered solution. This means that doping of solutions with nanoparticles affects nucleation in laser irradiation experiments, predominantly by their interaction with the laser. The results of filtration and doping with nanoparticles highly support the nanoparticle heating theory.

6.2 Recommendations

For conducting experiments with longer residence times, a number of recommendation can be given. First of all, sufficiently coating a 60 cm capillary might require further adjustments to the current protocol, this being a process of trial and error. Because such a process can be very time consuming, alternative coating techniques can be used to coat a 60 cm capillary. A second recommendation is to adapt the connection of the FEP tube coil to the capillary. This could be done by for example gluing the FEP tube coil to the capillary. However, this is not ideal as it allows for single time use of the FEP tube coil. Another way to adapt the connection is to use a square FEP tube that perfectly fits the size of the capillary. This reduces deformation of the FEP tube and might completely dissolve the problem of having back flow and dead zones.

Based on the results in Chapter 5, some follow-up experiments can be suggested in order to support the nanoparticle heating model. First, the influence of the nature of the nanoparticle on the nucleation probability and the crystal size can be investigated. The iron oxide nanoparticles

used in Chapter 5 give needle shaped crystals while a different type of nanoparticle might give another crystal habit. In addition, the size of the nanoparticle and corresponding agglomerates possibly plays a role in laser irradiation experiments as well. To find out if this is the case, laser irradiation experiments should be conducted with nanoparticles of the same type, but with a different nominal diameter. Furthermore, the concentration of nanoparticles in the solution should be investigated. With a nanoparticle concentration lower than that in Chapter 5, it is possible to observe nucleation probabilities below 100%. A set of experiments can be performed wherein a solution with a different nanoparticle concentration is used for each experiment. Finally the effect of common NPLIN parameters, such as laser intensity and wavelength, on nanoparticle doped solution can be explored as their effect is yet unknown.

Bibliography

[1] Andrew J. Alexander and Philip J. Camp. Single Pulse, Single Crystal Laser-Induced Nucleation of Potassium Chloride. *Crystal Growth Design*, pages 958–963, 2009.

[2] Andrew J. Alexander and Philip J. Camp. Non-photochemical laser-induced nucleation. *The journal of chemical physics*, 150, 2019.

[3] Daniel R. Cassar. Solving the classical nucleation theory with respect to surface energy. *Journal of Non-Crystalline solids*, 511:183–185, 2019.

[4] An-Chieh Cheng, Hiroshi Masuhara, and Teruki Sugiyama. Evolving Crystal Morphology of Potassium Chloride Controlled by Optical Trapping. *The Journal of Physical Chemistry C*, 124(12):6913–6921, 2020.

[5] Andre de Haan, Burak H. Eral, and Boelo Schuur. *Industrial separation processes*. 2020.

[6] Vincent J. de Munck. Non-photochemical Laser-Induced Nucleation of KCl from Aqueous solutions in a Droplet-Based Microfluidic System, 2021.

[7] Deniz Erdemir, Alfred Y. Lee, and Allan S. Myerson. Nucleation of Crystals from Solution: Classical and Two-Step Models. *Accounts of Chemical Research*, pages 621–629, 2009.

[8] B.A Garetz, Aber J.E., N.L. Goddard, R.G. Young, and A.S. Myerson. Nonphotochemical, Polarization-Dependent, Laser-Induced Nucleation in Supersaturated Aqueous Urea Solutions Crystallization from Solution. *Physiscal review letters*, 77(16):3475–3476, 1996.

[9] Rumen Georgiev, Uspal William E. Toscano, Sara O., and Huseyin B. Eral. Universal motion of mirror-symmetric microparticles in confined stokes flow. 2023.

[10] Ilse Gosens, Jan A. Post, Liset J.J. de la Fonteyne, Eugene H.J.M. Jansen, W. John Geus, Flemming R. Cassee, and Wim H. de Jong. Impact of agglomeration state of nano- and submicron sized gold particles on pulmonary inflammation. *Particle and Fibre Toxicology*, 7, 2010.

[11] N. Hidman, Gaetano Sardino, Dario Maggiolo, Henrik Ström, and Srdjan Sasic. Numerical Frameworks for Laser-Induced Cavitation: Is Interface Supersaturation a Plausible Primary Nucleation Mechanism? *Crystal Growth & Design*, 20(11):7276–7290, 2020.

[12] Nadeem Javid, Thomas Kendall, Ian S. Burns, and Jan Sefcik. Filtration Suppresses Laser-Induced Nucleation of Glycine in Aqueous Solutions. *Crystal Growth & Design*, 16(8):4196–4202, 2016.

[13] Young-Shin Jun, Jaguang Zhu, Jing Wang, Deoukchen Ghim, Xuanhao Wu, Doyoon Kim, and Haesung Jung. Classical and Nonclassical Nucleation and Growth Mechanisms for Nanoparticle Formation. *Annual Review of Physical Chemistry*, 73:453–477, 2022.

[14] Rohit Kacker, Sanjana Dhingra, Daniel Irimia, Murali K. Ghatkesar, Andrzej Stankiewicz, Herman J.M. Kramer, and Huseyin B. Eral. Multiparameter Investigation of Laser-Induced Nucleation of Supersaturated Aqueous KCl Solutions. *Crystal Growth and Design*, 18(1):312–317, 2018.

[15] J. Kardum and Aleksandra Sander. Batch Crystallization of KCl: the Influence of the Cooling and Mixing Rate on the Granulometric Properties of Obtained Crystals. *Chemical and Biochemical Engineering Quarterly*, 19, 2005.

[16] Demo Kashchiev. Classical nucleation theory approach to two-step nucleation of crystals. *Journal of Crystal Growth*, 530, 2020.

[17] Demo Kashchiev, Peter G. Vekilov, and Anatoly B. kolomeisky. Kinetics of two-step nucleation of crystals. *The Journal of Chemical Physics*, 122, 2005.

[18] B.C. Knott, Jerry L. LaRue, Alec M. Wodtke, Michael F. Doherty, and Baron Peters. Communication: Bubbles, crystals, and laser-induced nucleation. *The Journal of Chemical Physics*, 134, 2011.

[19] Vikram Korede, Nagaraj Nagalingam, Frederico M. Penha, Noah an der Linden, Johan T. Padding, Remco Hartkamp, and Huseyin B. Eral. A Review of Laser-Induced Crystallization from Solution. *Crystal Growth design*, 23(10):3873–3916, 2023.

[20] Vikram Korede, Nagaraj Nagalingam, Frederico M. Penha, Noah van der Linden, Johan T. Padding, Remco Hartkamp, and Huseyin B. Eral. A Review of Laser-Induced Crystallization from Solution. *Crystal Growth & Design*, 23(5):3873–3916, 2023.

[21] A.M. Mackenzie. *Investigating nucleation control in batch and flow using non-photochemical laser-induced nucleation*. PhD thesis, 2017.

[22] Johanna Midelet, Afaf H. El-Sagheer, Tom Brown, Antonios G. Kanaras, and Martinus H.V. Werts. The sedimentation of colloidal nanoparticles in solution and its study using quantitative digital photography. *Particle Particle System Characterization*, 34, 2017.

[23] Centro de Quimica Estrutural Molecular Energetics Group. Figure 1. Saturation-supersaturation diagram showing the stable, metastable, and labile zones for the crystallization of a solid from solution. The solid line represents the equilibrium solubility curve and the dashed line represents the maximum supersaturation or nucleation curve. The separation of the two curves represents the metastable zone width.

[24] Nagaraj Nagalingam, Aswin Raghunathan, Vikram Korede, Christian Poelma, Carlas S. Smith, Remco Hartkamp, Johan T. Padding, and Huseyin B. Eral. Laser-Induced Cavitation for Controlling Crystallization from Solution. https://arxiv.org/abs/2302.01218, 2023.

[25] Roberto Righini. Ultrafast Optical Kerr Effect in Liquids and Solids. *Science*, 262:1386–1390, 1993.

[26] Julien O. Sindt, Andrew J. Alexander, and Philip J. Camp. Structure and Dynamics of Potassium Chloride in Aqueous Solution. *The Journal of Physical Chemistry*, 118:94049413, 2014.

[27] Teruki Sugiyama and Shun-Fa Wang. Manipulation of nucleation and polymorphism by laser irradiation. *Journal of Photochemistry Photobiology, C: Photochemistry Reviews*, 52, 2022.

[28] Mias Veldhuis. Non-Photochemical Laser-Induced Nucleation, 2022.

[29] Jamieson Willam J. Ward, Martin R., Claire A. Leckey, and Andrew J. Alexander. Laser-induced nucleation of carbon dioxide bubbles. *Journal of Chemical Physics*, 142(14), 2015.

[30] Martin. R Ward, Alasdair M. Mackenzie, and Andrew J. Alexander. Role of Impurity Nanoparticles in Laser-Induced Nucleation of Ammonium Chloride. *Crystal Growth and Design*, 16, 2016.

[31] Julien Zaccaro, Jelena Matic, Allan S. Myerson, and Bruce A. Garetz. Nonphotochemical, Laser-Induced Nucleation of Supersaturated Aqueous Glycine Produces Unexpected -Polymorph. *Crystal Growth Design*, 1(1):5–8, 2001.

[32] Justin M. Zook, Vinayak Rastogi, Robert I. MacCuspie, Athena M. Keene, and Jeffrey Fagan. Measuring Agglomerate Size Distribution and Dependence of Localized Surface Plasmon Resonance Absorbance on Gold Nanoparticle Agglomerate Size Using Analytical Ultracentrifugation. *ACS Nano*, 5(10):8070–8079, 2011.

A

Appendix A

This section describes the procedures for coating 30 cm and 60 cm capillaries used in the experiments of chapters 3, 4 and 5.

A.1 Coating procedure for 30 cm capillaries

A square borosilicate capillary (30 cm, ID = 0.9 mm) is flushed with 10 ml 0.1 M NaOH solution and 2×10 ml ultra pure water respectively. After flushing, the inside of the capillary is dried with nitrogen, the outside is cleaned with a tissue. In a 5 ml vial, 16 µL of trichloro(1H,1H,2H,2H-perfluoroctyl)-silane is inserted with a micropipette. The vial is then closed and a hole is made in the lid of the vial. The capillary is inserted via this hole. The vial with the capillary is put inside a desiccator. In the same way as described above, 3 more capillaries are prepared, put in vials and placed in the desiccator. The desiccator is closed and subsequently the pressure inside the desiccator is reduced to 20 torr. The desiccator is left pressurized for at least 12 hours. The desiccator is opened by rotating the valve a little such that air gradually enters the desiccator. When the desiccator is back to standard pressure, it is opened and the capillaries are taken out of the vials. The capillaries are cleaned with aceton and a tissue from the outside.

A.2 Coating procedure for 60 cm capillaries

Attempts to coat 60 cm capillaries use the procedure in A.1 as slight variations on this procedure. Since 60 cm capillaries don't fit in a normal

desiccator, a custom built desiccator is made (see A.3). In a first attempt, the procedure of A.1 is followed completely. This leads to an insufficient coating and gives wetting issues while performing experiments. In a second attempt, the amount of trichloro(1H,1H,2H,2H-perfluoroctyl)-silane is doubled to 32 µL. Also, the amounts of of NaOH and ultra pure water are doubled to 20 ml and 2×20 ml respectively. This results in capillaries where the coating polymerised, visible as a white material stuck inside the capillary. The capillaries are considered to have too much coating and therefore are not usable in experiments. Since the amount of trichloro(1H,1H,2H,2H-perfluoroctyl)-silane is too much, an amount of 24 µL is used in a third attempt. Now the coating of the capillaries is insufficient. In a final effort, the pressure is lowered to 5 torr instead of 20 torr. This leads to varying results among the capillaries that are coated this way.

A.3 Self-made desiccator

Coating of a capillary with trichloro(1H,1H,2H,2H-perfluoroctyl)-silane is based on a pressure difference through the capillary. If the pressure at the top end of the capillary is lower than at the bottom end, the trichloro(1H,1H,2H,2H-perfluoroctyl)-silane travels trough the capillary from the higher to the lower pressure. At the wall of the capillary it will react with NaOH molecules, resulting in a layer of coating on the capillary wall. To create a large enough pressure difference, a desiccator is used wherein the pressure is lowered to near vacuum. A suitable desiccator that fits 60 cm capillaries is absent. Therefore a desiccator is made from PVC parts (see A.1). A PVC tube slightly higher than 60 cm is closed on one end with a cap and on the other end with a screw-able lit. In the lit, a hole is drilled such that it exactly fits a valve from a commercial desiccator. All PVC parts are glued together to prevent any leakages when keeping it at a near-vacuum.

Figure A.1: Custom built desiccator.

B

Appendix B

In this section, the protocols for preparing the solutions used in 3, 4, and 5 are presented.

B.1 Supersaturated KCl solutions

Clean a glass bottle(100 ml) suitable for storage, also clean a stirring bar. Add 27.62 g of KCl to a glass bottle. Subsequently add 70 ml of ultrapure water to the bottle. Put the stirring bar in the bottle, close it and seal the lit with parafilm to prevent loss of water via evaporation. Heat the solution at 60 °C on a heating plate and stir until all KCl is dissolved. This can take about 2 to 3 hours. Then put the bottle in the oven at 60 °C so that the solution can stabilize.

Instead of using a heating plate, one can use a sonicator to dissolve the KCl. To do so, put the KCl solution in the sonicator for 1 to 2 minutes at 50 °C. During those 1 to 2 minutes, stop the sonicator a few time and stir the solution by hand. When all KCl is dissolved, put the solution in the oven at 60 °C to stabilize.

B.2 Filtered KCl solutions

Put two syringes of 10 ml, two needles, a small piece of tubing and the desired filter in the oven at 60 °C. Prepare the KCl solution as in B.1 and store it in the oven at 60 °C for at least 10 minutes. Take the solution,

the syringe and the needle out of the oven. Fill the syringe with 10 ml of solution via the needle and attach a PTFE filter to the syringe. Now connect the tube to the filter and attach the other syringe to the tube. Slowly empty the first syringe into the second one. Wrap a piece of parafilm around the syringe and store it in the oven at 60 °C for at least 5-10 minutes before starting the experiment.

If a paper filter is desired, put the solution in a syringe via a needle. Remove the needle and put the paper filter on top of a beaker. Pour the solution on the paper filter and wait for all solution to pass through the filter. Attach the other needle to the second syringe and fill the syringe with the solution from the beaker. Cover the top of the syringe with parafilm and store it in the oven at 60 °C for at least 5-10 minutes before starting the experiment.

B.3 Supersaturated KCl solutions doped with nanoparticles

Clean a glass bottle (100 ml) suitable for storage and put it in the oven at 60 °C. Also put seven syringes, needles and PFTE filters with a pore size of 0.45 μm in the oven. Prepare the KCl solution as in B.1. Fill a syringe with solution via the needle, disconnect the needle and attach a filter. Take the bottle out of the oven and push the solution through the filter in the bottle. Repeat this for all the other syringes, needles and filters.

Add 0.00118 g of iron oxide nanoparticles (50-100 nm nominal diameter) to 33 ml of ultrapure water in a plastic tube. Shake the solution for approximately 10 seconds. Put a sonicator horn inside the tube and place a beaker filled with cold water around the tube to prevent the nanoparticle suspension from heating up. Turn on the sonicator for 3 hours, with breaks of 10 seconds every 1 minute. This prevents overheating of the solution and the sonicator horn. After sonication, heat a sonicator bath to 50°C and take the filtered KCl solution out of the oven. Fill a 2 ml syringe with nanoparticle suspension via a needle add 1.5 g of the nanoparticle suspension to the solution. Put the solution in the sonicator bath at 50 °C for and turn on the desiccator for a few seconds. Store the solution in the oven for at least 5 to 10 minutes, before filling a syringe with the solution.

C

Appendix C

C.1 Experimental procedure

This section describes the experimental procedure for the experiments that are performed in Chapter 4 and Chapter 5.

C.1.1 Before the experiment

- Turn on the hairdryer that is connected to an arduino and a relay model to keep the temperature stable around 40 °C. Now open the code for the hairdryer in order to verify the temperature during the experiment.
- Fill a 10 ml syringe with demineralised water and a 20 ml syringe with silicon oil (10 cst). Put both syringes in the microfluidic pumps inside the temperature controlled environment for at least 40 minutes such that they heat up to 40 °C. Prepare a second 20 ml syringe with oil and put keep it aside in the box.
- Cut a small piece of PTFE tubing and put it almost entirely over one end of the capillary (square, ID = 0.9 mm). Subsequently put a cap over the tube, make sure the tube is not allth way in.
- Put a ferrule around the tube on the capillary such that it touches the cap. Now screw the capillary in a t-junction. When placed horizontally on a surface, the capillary should be parallel to the surface.

- Take an inner capillary (5 cm) and use sanding paper to make a small hole at the end of the inner capillary. Slowly insert the inner capillary in the mixing zone until it won't go any further. Put the other end in the t-junction of the capillary and screw the mixing zone in the t-junction.
- Put the mixing zone with the capillary in the temperature controlled environment and move the capillary through the opening of the environment such that it is resting on the iron railing.
- Connect the oil tube to the t-junction and then connect the water syringe and oil syringe to the mixing zone and the oil tube respectively.
- Take two plastic holders and put them around the capillary so that the capillary is straight on the railing. For extra support, put a magnet on the railing against one of the holders.
- Open the viewing software, turn on the camera and the LED, make sure that the capillary is clearly visible in the viewing software.
- Put a copper wire standing in a beaker to the end of the capillary. The copper wire will guide the droplets from the capillary to the beaker and therefore reduces the chance of clogging.
- Turn on the oil pump for 2 minutes with a flow rate of 500 μL/min. Then turn on the water pump for 2 minutes at a flow rate of 310 μL/min. Now reduce the flow rate of the water pump to 10 μL/min and wait 1 minute. Finally, reduce the flow rate of the oil pump to 100 μL/min. Wait for 15 minutes. Within this time, the droplets should stabilize and become almost uniform.
- Stop the water pump and wait for all water to leave the mixing zone and the capillary before stopping the oil pump as well. Take out both syringes and put the new syringe with oil in the microfluidic pump.
- For a laser irradiation experiment, turn on the laser. With a laser detection card, mirror and lenses, direct the laser to the right spot on the capillary. Measure the power of the laser. The power should be approximately 50 MW/m^2. Now close the laser, but don't turn it off.

C.1.2 The experiment

- Fill a 10 ml syringe with the solution by using a needle (both the syringe and the needle should be preheated. Cover the end of the syringe with parafilm and put it in back in the oven for 5 minutes
- Take the syringe out of the oven and place on the microfluidic pump. Now wait for 2 minutes.
- Turn on the oil pump for 2 minutes with a flow rate of 500 μL/min. Then turn on the solution pump for 2 minutes at a flow rate of 310 μL/min. Now reduce the flow rate of the solution pump to 10 μL/min and wait 1 minute. Finally, reduce the flow rate of the oil pump to 100 μL/min. Wait until stable droplets are observed.
- If the laser is on, open the laser and wait 2 minutes.
- Start recording the experiment and wait until 1000-1200 droplets have passed the camera. Stop recording.

C.1.3 After the experiment

- Close the laser, stop the pumps, turn off the camera and the LED and disconnect the hairdryer.
- Replace the syringe with solution by a syringe of demineralised water and turn on the water pump and the oil pump at 310 μL/min and 500 μL/min to flush the mixing zone and the capillary.
- Disassemble all parts within the microfluidic setup and wash the ferrule, t-junction and the mixing zone with demineralised water before drying them with air. Turn off the laser completely.
- Play the recording and manually count the total number of droplets and the number of droplets that contain at least 1 crystal in order to get the nucleation probability. Manual counting can be verified with a counting code based on machine learning.